NOTES AND CORRESPONDENCE

Application of Satellite-Derived Atmospheric Motion Vectors for Estimating Mesoscale Flows

KRISTOPHER M. BEDKA

Cooperative Institute for Meteorological Satellite Studies, Space Science and Engineering Center, University of Wisconsin—Madison, Madison, Wisconsin

JOHN R. MECIKALSKI

Atmospheric Science Department, The University of Alabama in Huntsville, Huntsville, Alabama

(Manuscript received 9 August 2004, in final form 14 February 2005)

ABSTRACT

This study demonstrates methods to obtain high-density, satellite-derived atmospheric motion vectors (AMV) that contain both synoptic-scale *and* mesoscale flow components associated with and induced by cumuliform clouds through adjustments made to the University of Wisconsin—Madison Cooperative Institute for Meteorological Satellite Studies (UW-CIMSS) AMV processing algorithm. Operational AMV processing is geared toward the identification of synoptic-scale motions in geostrophic balance, which are useful in data assimilation applications. AMVs identified in the vicinity of deep convection are often rejected by quality-control checks used in the production of operational AMV datasets. Few users of these data have considered the use of AMVs with ageostrophic flow components, which often fail checks that assure both spatial coherence between neighboring AMVs and a strong correlation to an NWP-model first-guess wind field. The UW-CIMSS algorithm identifies coherent cloud and water vapor features (i.e., targets) that can be tracked within a sequence of geostationary visible (VIS) and infrared (IR) imagery. AMVs are derived through the combined use of satellite feature tracking and an NWP-model first guess. Reducing the impact of the NWP-model first guess on the final AMV field, in addition to adjusting the target selection and vector-editing schemes, is found to result in greater than a 20-fold increase in the number of AMVs obtained from the UW-CIMSS algorithm for one convective storm case examined here. Over a three-image sequence of *Geostationary Operational Environmental Satellite* (*GOES)-12* VIS and IR data, 3516 AMVs are obtained, most of which contain flow components that deviate considerably from geostrophy. In comparison, 152 AMVs are derived when a tighter NWP-model constraint and no targeting adjustments were imposed, similar to settings used with operational AMV production algorithms. A detailed analysis reveals that many of these 3516 vectors contain low-level (100–70 kPa) convergent and midlevel (70–40 kPa) to upper-level (40–10 kPa) divergent motion components consistent with localized mesoscale flow patterns. The applicability of AMVs for estimating cloud-top cooling rates at the 1-km pixel scale is demonstrated with excellent correspondence to rates identified by a human expert.

1. Introduction

Satellite-derived winds [or atmospheric motion vectors (AMV)] are produced from all operational geostationary satellites and have been since the 1960s (Fujita 1968; Hubert and Whitney 1971). Common techniques in use today are described by Velden et al. (1997, 1998) for the Geostationary Operational Environmental Satellite (GOES) series (Menzel and Purdom 1994), by Schmetz et al. (1993) for the European Meteosat, and by Tokuno (1996) and LeMarshall et al. (1999) for the Japanese Geostationary Meteorological Satellite (GMS). Satellite-derived AMVs have recently been produced using Moderate-Resolution Imaging Spectro-

Corresponding author address: Kristopher M. Bedka, Cooperative Institute for Meteorological Satellite Studies, Space Science and Engineering Center, University of Wisconsin—Madison, 1225 West Dayton St., Madison, WI 53706-1695.
E-mail: kristopher.bedka@ssec.wisc.edu

radiometer (MODIS) instrument data for the polar latitudes, where image frequencies are on the order of ~1 h (Key et al. 2002). Nieman et al. (1997) and Velden et al. (1998) outline the development of fully operational, automated winds from the *GOES-8/-9* sensors within the National Environmental Satellite, Data, and Information Service (NESDIS).

AMVs are widely used in a variety of weather analysis and prediction (e.g., Velden and Young 1994; Schmetz et al. 1995; Sakamoto et al. 2004), data assimilation (LeMarshall et al. 1996; Goerss et al. 1998; Soden et al. 2001; Xiao et al. 2002; Bonavita and Torrisi 2004; Cherubini et al. 2004), and tropical cyclone research applications (Velden et al. 1992, 1998; Dunion and Velden 2002). The World Meteorological Organization (WMO)-sponsored International Winds Workshop proceedings from the sixth and seventh workshops in 2002 and 2004, respectively, provide a sound background into the wide applicability of these data.

The purpose of this note is to describe the use of satellite-derived AMVs for the identification of motions associated with and induced by convective clouds (meso-γ and meso-β scales, in particular: scales from 2 to 200 km) for which information about ageostrophic flow is important. Satellite AMVs that contain significant mesoscale flow components are often rejected by quality-control checks within the processing algorithm using a typical operational methodology tuned for larger-scale, geostrophically balanced flow depiction. Convectively induced motions are one example of flows that can deviate greatly from geostrophic balance, often leading to rejected AMVs. High-density "mesoscale" AMVs can directly identify ageostrophic flow patterns associated with and induced by moving convection in near–real time. Other methods for cloud motion assessment such as Lagrangian flow models require an accurate knowledge of the three-dimensional atmospheric mass distribution, which can only be identified through computationally expensive, high-resolution, cloud-resolving model simulation.

This note demonstrates a technique to obtain high-density mesoscale AMVs, using the University of Wisconsin—Madison Cooperative Institute for Meteorological Satellite Studies (UW-CIMSS) processing algorithm (Velden et al. 1997, 1998), that contain valuable information for a variety of subsynoptic-scale meteorological applications. As proof of their value, these mesoscale AMVs are applied to help to estimate cumulus-cloud growth rates. Section 2 outlines methods that allow for the identification of mesoscale AMVs using the UW-CIMSS algorithm. Section 3 provides an example on the use of such information within a technique that nowcasts convective initiation (CI) using geostationary satellite data. Section 4 summarizes the findings.

2. Method

Normal operational procedures used to obtain AMVs from sequences of GOES satellite images are described in detail within Velden et al. (1997, 1998). A brief description of this satellite AMV identification algorithm is provided as follows. After initial image registration and navigation checks are performed, "targets" are identified that can be effectively tracked across a sequence of geostationary satellite images with relatively high time resolution ($\leq$1 h between images). GOES satellite information used in the AMV targeting scheme includes visible (VIS) brightness counts (0.65 μm) and brightness temperatures from the 3.9- [shortwave infrared (SWIR); Velden et al. 2005], 6.5- [water vapor (WV)], and 10.7- (IR) μm channels. Suitable targets represent well-defined cloud features (VIS, SWIR), coherent cloud edges (VIS, SWIR), or brightness temperature (T_B) gradients in the WV channel. AMVs are computed by identifying and tracking these targets across an image sequence through the use of advanced pattern-matching techniques based on cross-correlation statistics (Merrill et al. 1991). One of several IR satellite-based techniques, such as the carbon dioxide (CO_2)-slicing algorithm (Menzel et al. 1983) or the water vapor (H_2O)-intercept method (Szejwach 1982; Nieman et al. 1997), is selected by a hierarchical scheme within the algorithm for AMV height assignment (Velden et al. 1998).

The AMVs are then passed through editing and quality-control routines. These routines check the overall coherence of the AMV field [the quality indicator (QI) technique; Holmlund 1998] and the fit of each individual vector to an NWP first-guess wind field [recursive filter (RF) analysis; Hayden and Purser 1995]. In typical operational AMV processing schemes, adjustable quality-control settings within the algorithm require AMVs to meet nearest-neighbor coherence checks. Those AMVs that differ greatly from neighboring vectors or deviate from the first guess are typically assigned low QI and RF analysis scores. AMVs with low scores (e.g., less than 60 out of 100 for the QI analysis) are typically "blacklisted" from operational NWP global data assimilation because they are believed to contain little useful information.

A detailed analysis reveals that many operational AMVs with low QI and RF scores are indeed depictions of actual atmospheric flow and can be associated with motions induced by convective clouds (Mecikalski 2002; Rabin et al. 2004). These AMVs often represent

ageostrophic or accelerating divergent (convergent) flow associated with anvil-level outflow (boundary layer inflow). They are screened out of typical operational satellite AMV datasets because the NWP model either cannot simulate convective storm development in the correct location or cannot accurately resolve and represent the complex flow associated with and induced by convective clouds on the meso-γ (subgrid) and meso-β scales. Therefore, AMVs induced by convective clouds are treated as "noise" within operational AMV processing because they do not correlate well with the geostrophically balanced synoptic-scale flow represented in the NWP-model first-guess wind field.

To ameliorate this concern, a processing technique is developed in an effort to obtain high-density VIS, IR, and WV AMVs that contain contributions from *both* the synoptic scale and mesoscale. The technique involves simple modifications to the UW-CIMSS processing scheme. First, the size of the AMV target box is reduced from the default size of 15 $\times$ 15 pixels to 5 $\times$ 5 pixels [$\sim$1- (VIS) and $\sim$4- (IR) km resolution per pixel]. VIS targets are tracked throughout the entire depth of the troposphere and lower stratosphere (100–10 kPa); this tracking differs from operational settings in which targets are only identified in the lower troposphere to midtroposphere (100–60 kPa). Also, the maximum IR target T_B was increased from 250 to 285 K to allow tracking of lower-tropospheric cumulus clouds. The goal of these steps is to increase the number of targets for subsequent tracking, which will therefore increase the density of the resulting AMV field. Second, the impact of the NWP first guess on the resulting AMV field is greatly down-weighted through a reduction of the minimum required QI [25 vs 60 (operational)] and RF [0.01 vs 0.90 (operational)] analysis score thresholds. In addition, gross error checks that penalize directional and speed variations from the background guess field (typically 90° and 10 m s^{-1}) are turned off to minimize further the impact of the first guess on the final satellite-derived AMV field.

The following section describes the value of AMVs using the aforementioned processing changes to obtain AMVs that describe mesoscale flow within an application that nowcasts initial convective storm formation. We will refer to these AMVs as mesoscale, given their ability to describe unbalanced flows and divergent circulations.

3. Application of mesoscale AMVs

Mecikalski and Bedka (2005, hereinafter MB05) outline an algorithm for the real-time prediction of CI at lead times from 30 min to 1 h. The UW-CIMSS AMV algorithm is used within the CI nowcast system with the adjustments described above to derive AMVs that describe cloud-scale motion, expansion, and local convergent/divergent flows important for maintaining cumulus growth. Within this system, there is a heavy reliance on the use of mesoscale AMVs for tracking cumulus in 5–15-min-temporal-resolution *GOES-11* and *GOES-12* imagery so that temporal changes of IR cloud characteristics may be monitored.

For this application, satellite-offset vectors (SOV) are formed for cumulus clouds using mesoscale AMVs to track the movement of cumulus clouds and to assess cloud-top trends between successive GOES images. An SOV is defined as the number of 1-km pixels in the latitudinal/longitudinal direction for which a given cumulus cloud pixel has moved in the time interval between two satellite images. The SOV is calculated by 1) decomposing the AMV speed and direction into u (zonal) and v (meridional) components, 2) multiplying the u and v wind components by the time interval between images, and 3) dividing this quantity by the pixel resolution to obtain the number of pixels in the u and v directions by which a cloud feature has moved between images. In knowing this information, we can derive cloud-top IR trends by taking the difference between IR T_Bs at the current pixel location and those at the SOV-derived past location.

The calculation of mesoscale AMVs for use within the CI nowcast algorithm incorporates three consecutive satellite images (from $t_1 = 0$ to $t_3 = t_1 - 30$ min) from the GOES 1-km VIS and the 4–8-km 6.5–6.7-μm WV and 10.7-μm IR window channels. Once the AMVs are obtained, a Barnes (1964) objective analysis is performed to produce an AMV analysis at the 1-km VIS resolution for three atmospheric layers: 100–70, 70–40, and 40–10 kPa. These broad atmospheric layers are selected to account for errors in AMV height assignment by the UW-CIMSS algorithm (Rao et al. 2002). GOES IR imagery is interpolated to the 1-km VIS resolution to allow for the combined use of VIS and IR analysis techniques at each VIS pixel, thereby preserving the enhanced spatial detail of the GOES VIS channel. Pixels classified as cumulus clouds by a VIS/IR cumulus cloud mask (described in MB05) are assigned an AMV from one of these three layers, depending upon the relationship between the pixel 10.7-μm T_B and an NWP model [the National Centers for Environmental Prediction North American Mesoscale (formerly Eta) Model] temperature profile. Cloud-top trends are calculated only if an AMV is present at the appropriate height within the vicinity of a cumulus cloud ($\sim$0.25° radius).

After determining the SOV-derived past pixel location, a check is performed to ensure that the past pixel

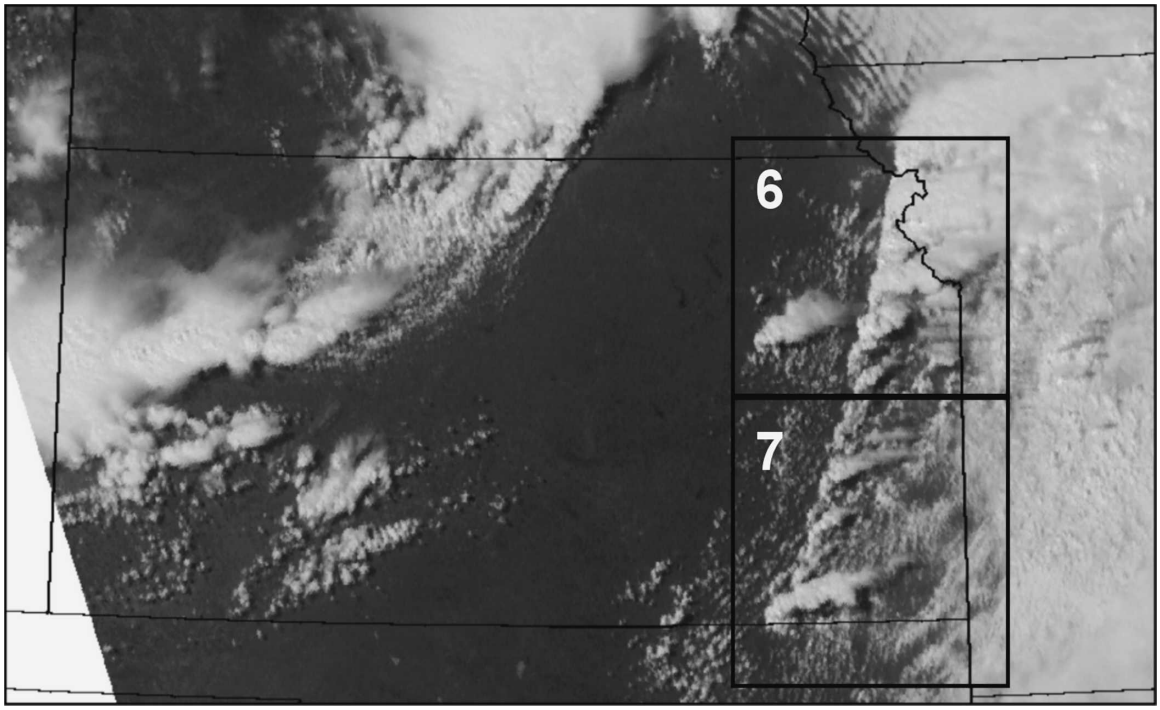

FIG. 1. A 1-km-resolution *GOES-12* visible image at 2002 UTC 4 May 2003. Highlighted in black boxes are regions featured in Figs. 6 and 7.

does indeed represent a cumulus cloud. Assuming that a pixel passes both checks (AMV availability and past cumulus cloud presence) for both the 5- (15-) and 10- (30-) min time lags of *GOES-11* (*GOES-12*) imagery, cloud-top cooling and multispectral band difference trends are calculated (see MB05). The passage of these checks indicates that a cumulus cloud is being tracked, back to a reasonable prior location, across successive images.

Errors in estimating cloud-top T_B trends using AMVs are inevitable, despite use of the above checks and every effort made to obtain accurate vectors in terms of direction and magnitude. Because quality-control checks have been greatly relaxed within the UW-CIMSS algorithm, incorrect vectors are occasionally derived and can result in grossly unreasonable cloud-top T_B trends. The aforementioned cumulus-cloud tracking checks are designed to minimize the impact of errant AMVs on trend calculations but are by no means perfect in filtering out all effects of these vectors. Nonetheless, SOVs obtained from satellite-derived AMVs are perhaps the only means of tracking clouds with reasonable accuracy over large geographical regions in real time, thereby offering a substantial improvement over a simple per-pixel differencing technique that does not take cloud motion into account (see MB05 for a comparison of these two techniques).

Figure 1 shows a *GOES-12* 1-km visible image at 2002 UTC 4 May 2003 as convective storms were rapidly developing across Kansas. For this event, a strong, slow-moving spring storm served as the focal point for a severe thunderstorm outbreak across much of the U.S. southern plains. Figure 2 shows *GOES-12* 4-km 10.7-μm IR imagery at 1932 (Fig. 2a) and 2002 (Fig. 2b) UTC and highlights the locations of rapidly growing cumulus clouds.

Figures 3–5 demonstrate AMVs derived using a sequence of three 15-min-resolution images from 1932 to 2002 UTC. An important increase in the number of AMVs derived from this image sequence occurs when the aforementioned adjustments are applied to the UW-CIMSS algorithm over those derived using typical operational settings. Over the entire domain shown in Figs. 3a, 4a, and 5a, 152 AMVs are produced when larger AMV targeting boxes and a stricter editing method is used. In contrast, 3516 AMVs are produced when the algorithm settings are adjusted in the manner described in section 2 (Figs. 3b, 4b, and 5b). AMVs within the 100–70-kPa layer (1178 vectors) are used for tracking of immature, nonprecipitating cumulus, whereas AMVs within the 70–40- (1283 vectors) and 40–10- (1055 vectors) kPa layers are used for tracking newly developing and mature cumulus, respectively. Vectors derived from the VIS channel (3212 vectors)

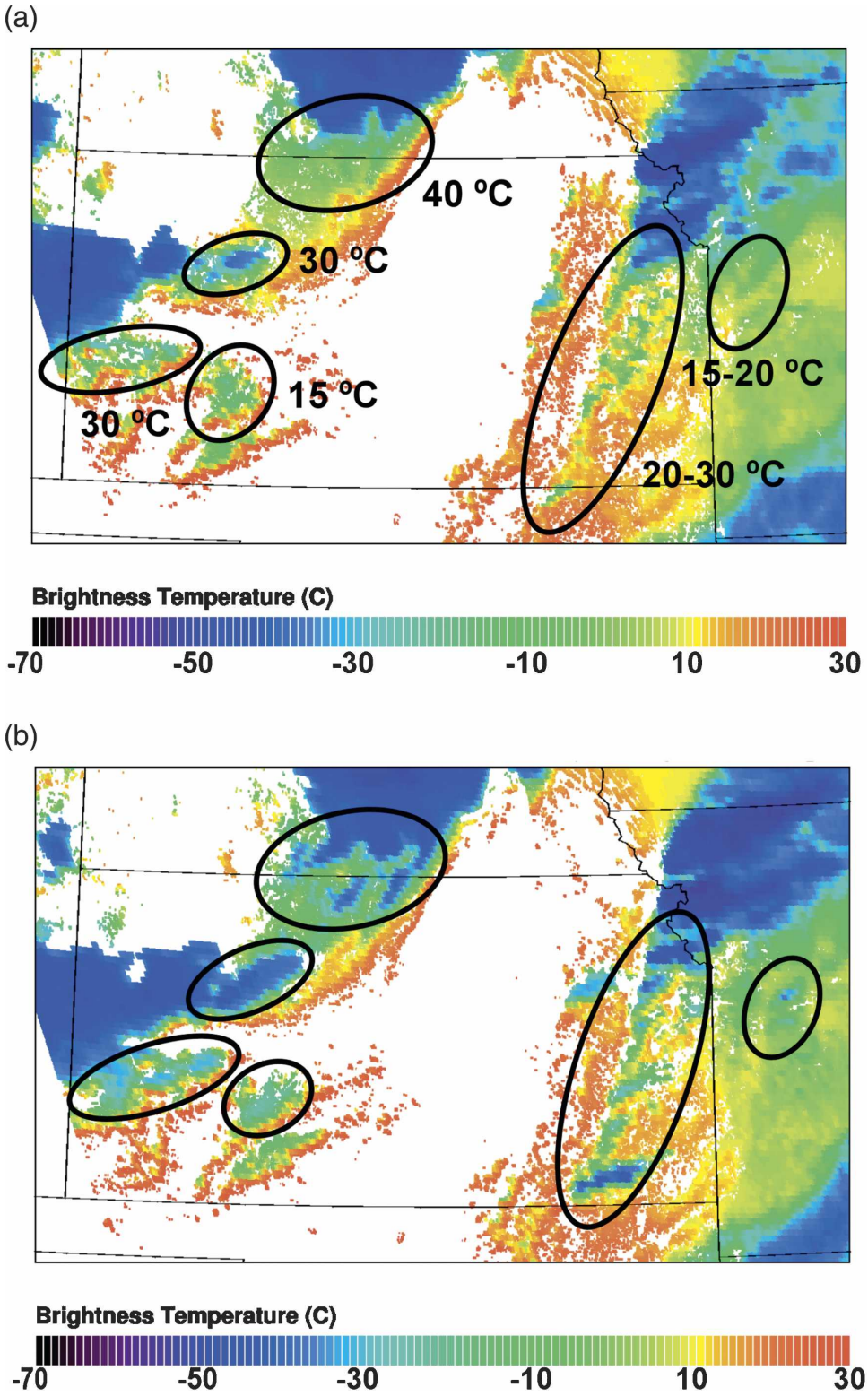

FIG. 2. *GOES-12* color-enhanced 10.7-μm imagery at (a) 1932 and (b) 2002 UTC 4 May 2003. Developing convection is outlined by ovals, and the mean 30-min temperature decrease (determined by a human expert) is listed for each distinct growing cumulus cluster in (a).

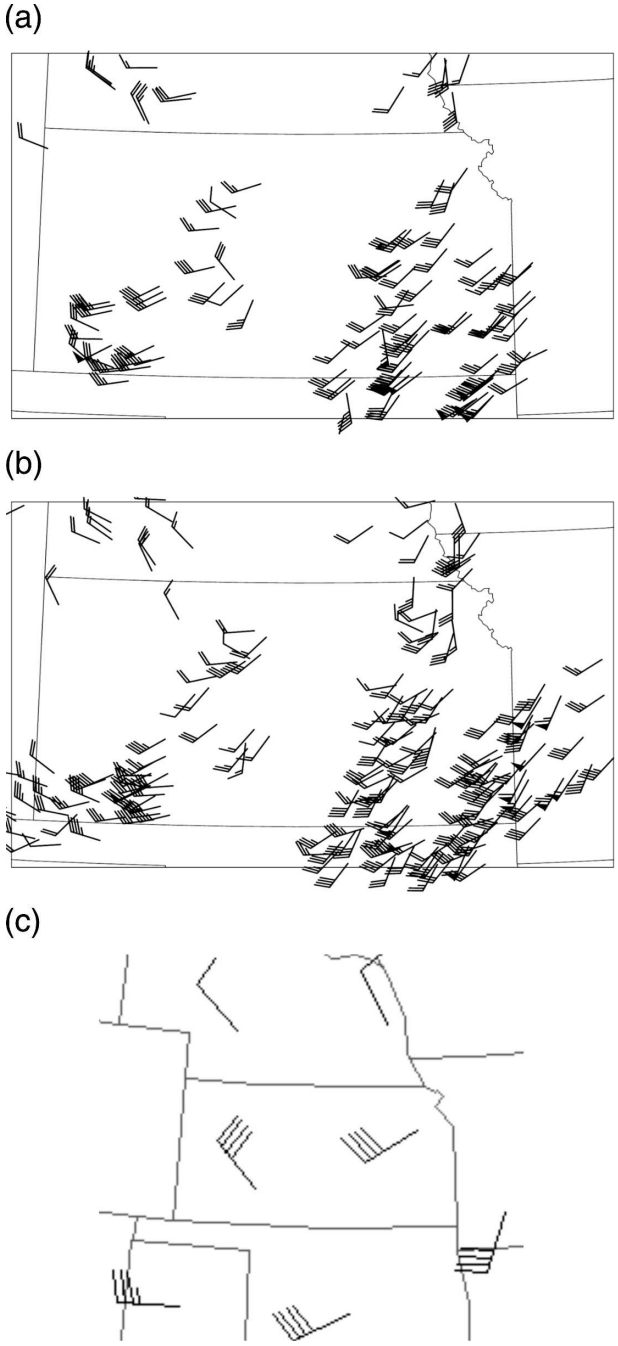

FIG. 3. (a) AMVs (kt; 1 kt = 0.5144 m s^{-1}) within the 100–70-kPa layer at 2002 UTC 4 May 2003 using a typical operational processing methodology. (b) AMVs for which the background wind field is down-weighted, allowing for synoptic- and mesoscale flows (so called mesoscale AMVs in the text). For clarity, only 20% of the mesoscale AMVs are randomly selected for display, whereas all AMVs in (a) are displayed. (c) The 85-kPa radiosonde wind observations (kt) at 0000 UTC 5 May 2003 for comparison with the satellite AMVs. Note that the radiosonde observations were collected 4 h later than the AMV field.

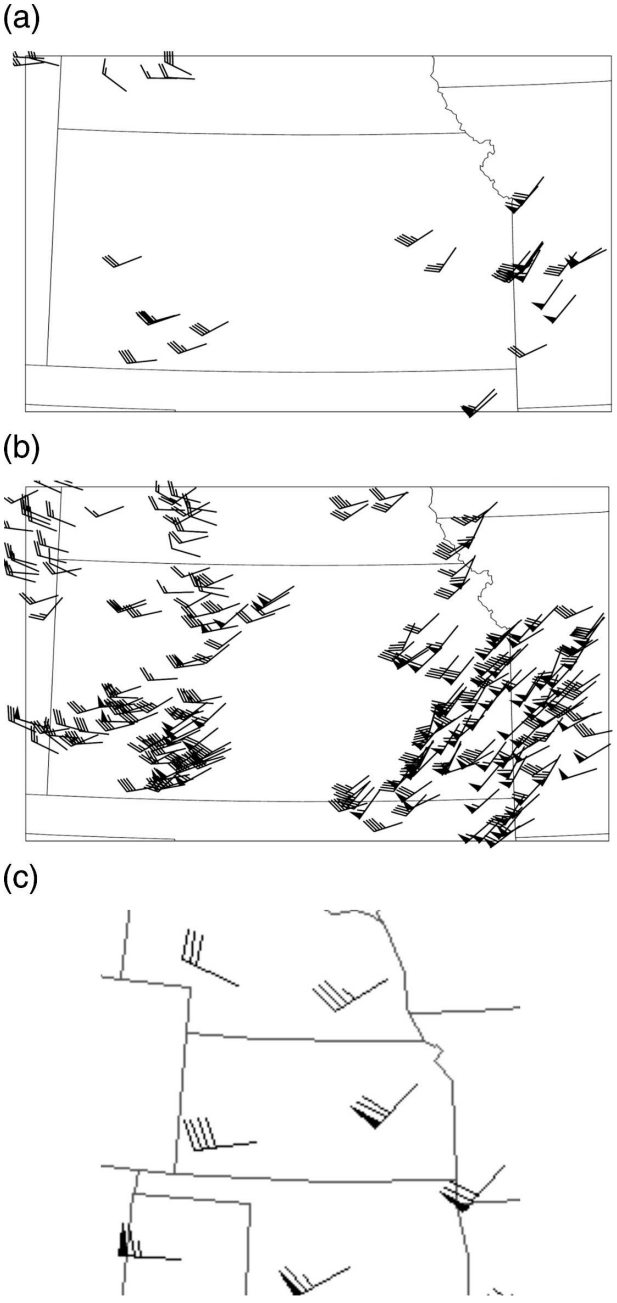

FIG. 4. (a), (b) The same as in Fig. 3, but for the 70–40-kPa layer. (c) The 50-kPa radiosonde wind observations at 0000 UTC 5 May 2003.

outnumber those from the WV and IR channels (304 vectors) by a factor of greater than 10, thereby demonstrating the importance of high-resolution 1-km imagery for mesoscale flow depiction. A comparison between the mesoscale AMV field and regional radiosonde observations (Figs. 3c, 4c, and 5c) indicates that the vast majority of the mesoscale AMVs possess reasonable speed and direction within all three atmo-

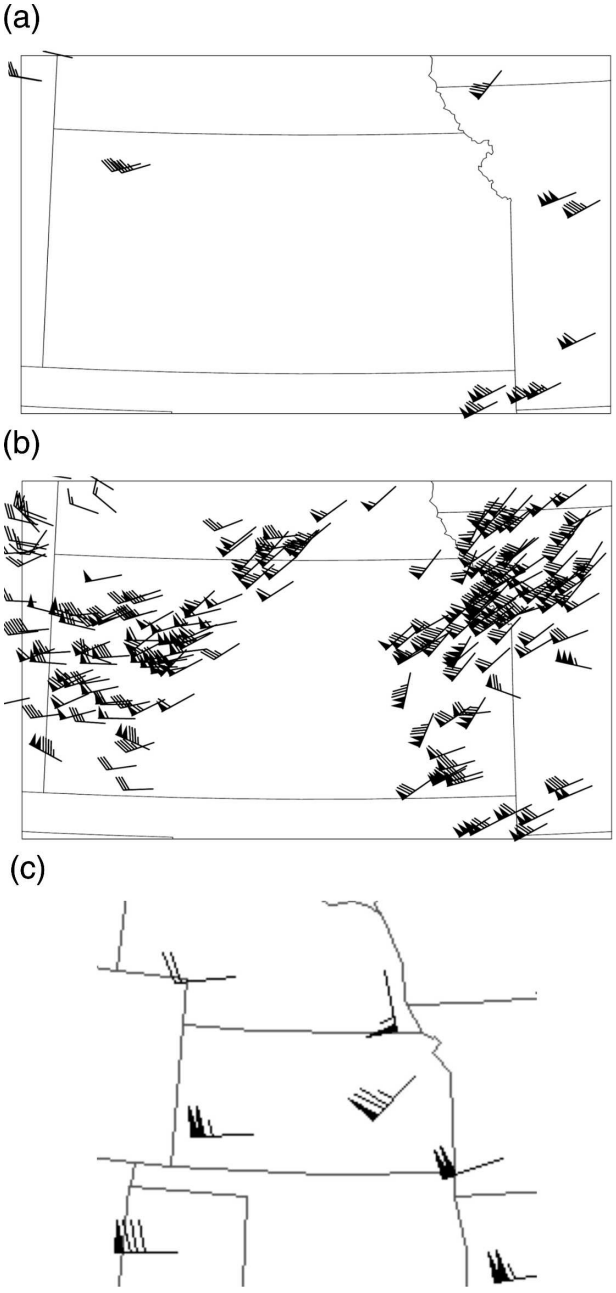

FIG. 5. (a), (b) The same as in Fig. 3, but for the 40–10-kPa layer. (c) The 25-kPa radiosonde wind observations at 0000 UTC 5 May 2003.

spheric layers, given the caveats that the radiosonde observations were collected 4 h later than the AMVs and that weather balloons are moving measurement platforms that are advected away from the launch location during ascent.

A closer examination of the mesoscale AMV field over a limited domain demonstrates the ability of this processing technique to retrieve detailed atmospheric flow in the vicinity of convective clouds. Figure 6 shows a combination of VIS imagery and the mesoscale AMV field in northeast Kansas. As expected, the AMVs within the 40–10-kPa layer correlate well with mature convection and cirrus anvil clouds. Divergent flow is apparent within the deep convection and cirrus anvil extending from extreme northeastern Kansas into Missouri. Several AMVs with speeds of more than 100 kt (1 kt = 0.5144 m s^{-1}) are present, which is indicative of flow at or above the 25-kPa level (see Fig. 5c). Diffluent flow is apparent within the 70–40-kPa AMV field at the periphery of the deep convection. Intense midtropospheric and upper-tropospheric diffluence was noted as one of the primary mechanisms in initiating convective storm development and maintaining storm intensity during this event. (M. Kruk, Midwestern Regional Climate Center, 2005, personal communication). Lower-tropospheric convergence is evident in the AMV field within the domain shown in Fig. 7 and yet is masked to a degree by the fact that most AMVs in the vicinity of the cumulonimbus and taller cumulus clouds apply to levels above 70 kPa. Several vectors with assigned heights lower than 90 kPa are outlined in boxes and illustrate the convergence of southerly flow ahead of the primary cloud line with west-southwesterly flow behind the line. This convergence later contributed to storm development in southeastern Kansas and northern Oklahoma. AMVs as shown in Figs. 6 and 7 are critical for forming SOVs within the CI nowcasting algorithm of MB05 because they are at a density that is meaningful to the study of meso-γ–meso-β-scale phenomena.

A 30-min cloud-top cooling estimate using both operational and mesoscale AMVs is presented in Fig. 8. Roberts and Rutledge (2003) noted that a drop in the satellite-detected 10.7-μm T_B from $\geq 0°$ to $\leq -20°$C and cooling rates of $-8°$C over 15 min (their "vigorous growth" criteria) are important precursors to storm initiation for the cases examined in their study. Through a detailed comparison of satellite cloud-growth trends and corresponding radar imagery, MB05 incorporate 10.7-μm and multispectral T_B band differencing temporal trends as 62.5% (5 of 8) of the criteria within their nowcasting system because of the high correlation of these trends with the CI process. Therefore, T_B trends calculated using mesoscale AMVs must be accurate because of the importance of these fields for CI nowcasting.

The use of operational AMV algorithm settings yields vector densities that are inadequate for use in the MB05 CI nowcasting application. A comparison of Fig. 8a with Fig. 2a indicates that the vast majority of convective development is not captured when operational

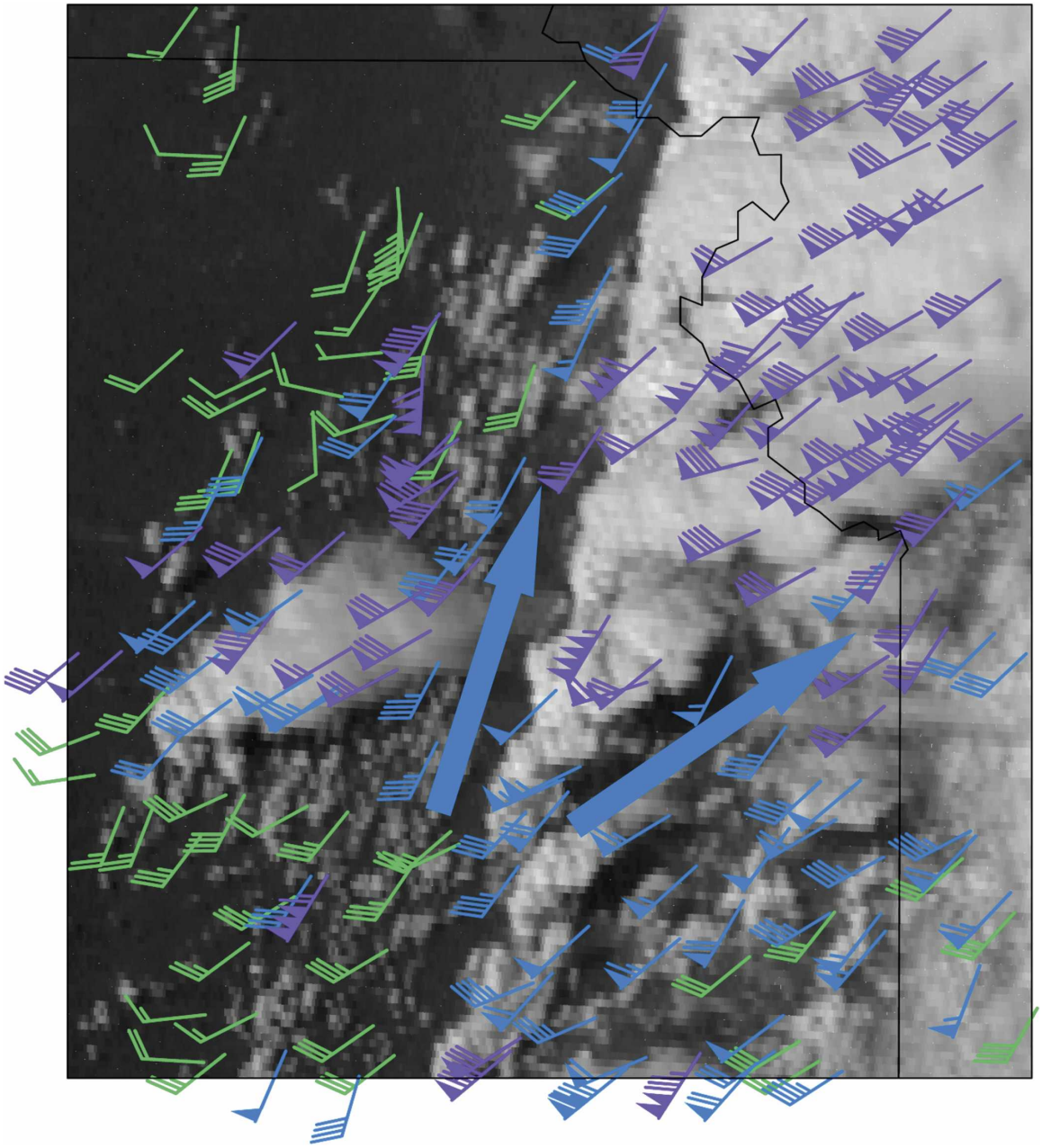

FIG. 6. Mesoscale AMVs laid over *GOES-12* VIS brightness centered on developing convection over northeast Kansas at 2002 UTC. Green barbs represent AMVs within the 100–70-kPa layer, blue AMV barbs are within the 70–40-kPa layer, and purple AMV barbs are within the 40–10-kPa layer. Blue arrows highlight midtropospheric diffluence in the vicinity of the mature convection. For clarity, only 50% of the AMVs are randomly selected for display.

vectors are used. Because operational AMVs are numerous within the 100–70-kPa layer (Fig. 3a), cooling rates associated with small, immature cumulus dominate the cloud-top cooling field. The number of AMVs is substantially lower within the 70–40- and 40–10-kPa layers, primarily resulting from that fact that VIS AMVs are only computed at levels below 60 kPa in operational AMV algorithms. Being that VIS AMVs greatly outnumber WV and IR vectors for this case and are not computed at levels above 60 kPa, cooling rates are not calculated for newly developing midlevel cumulus nearing the MB05 CI criteria.

In contrast, a comparison of Fig. 8b with Fig. 2a reveals that accurate cooling estimates can be calculated

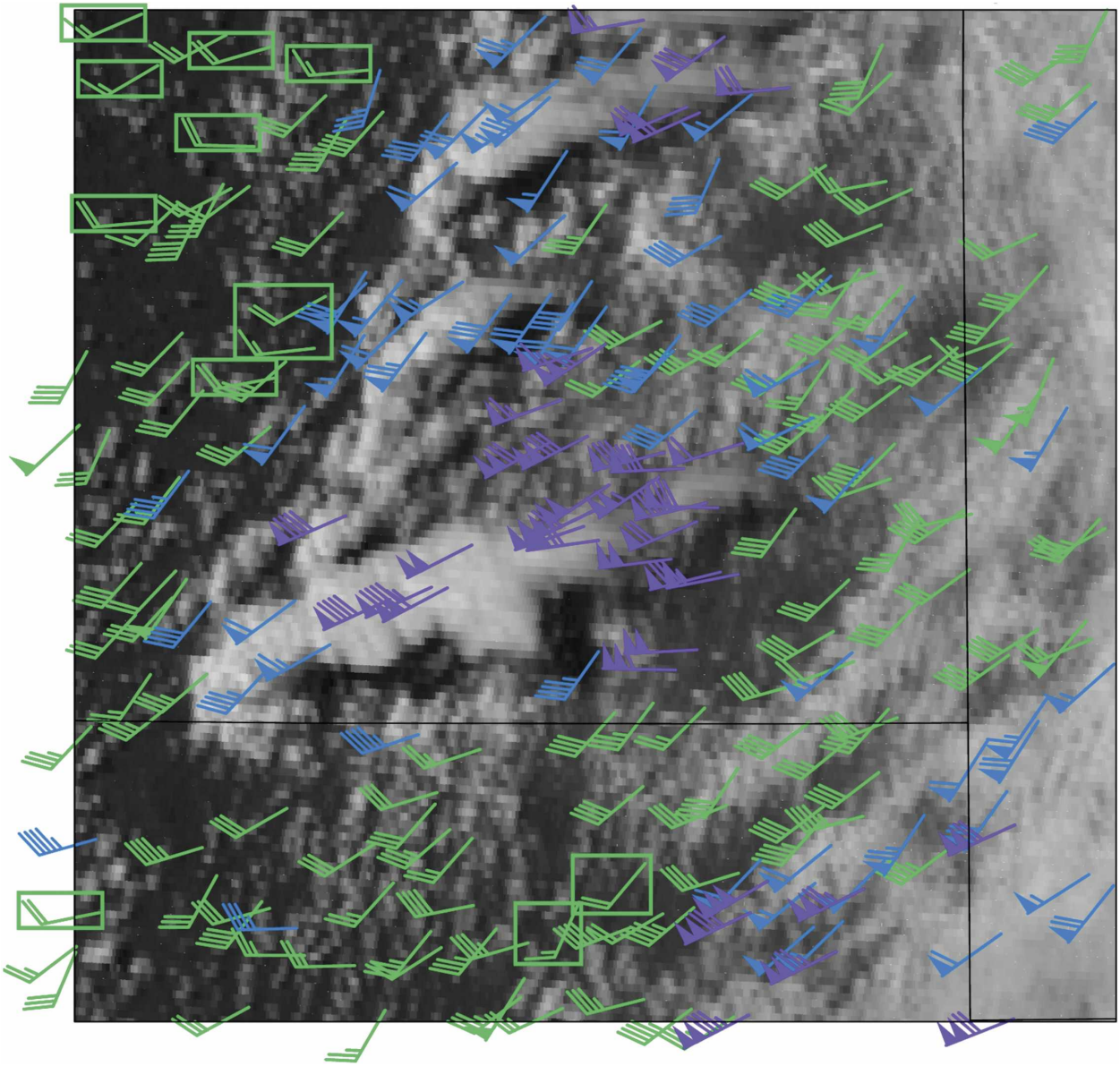

FIG. 7. Mesoscale AMVs laid over *GOES-12* VIS brightness centered on a combination of growing immature/mature convection over southeast Kansas. Green barbs outlined by boxes illustrate convergent flow at levels below 90 kPa. Barb color and density are the same as in Fig. 6.

using mesoscale AMVs. MB05 show that CI in west-central and eastern Kansas can be nowcast up to 45 min in advance through the proper identification of the vigorous cooling rates [20°–30°C (30 min)$^{-1}$] present in these locations. Isolated locations of intense convective growth [30°–40°C (30 min)$^{-1}$] are also identified within the domain shown in Fig. 6, as well as in north-central and southwest Kansas. Therefore, based on the high quality of the trend estimates shown by comparison of Figs. 2a and 8b, it is felt that the mesoscale AMVs are valuable within applications that require high-resolution momentum information on subsynoptic spatial and temporal scales.

4. Summary

This note outlines the modifications made to the UW-CIMSS satellite-derived AMV identification algorithm to obtain high-density AMVs that contain contributions from both synoptic-scale *and* mesoscale flows. Such mesoscale flows typically are not in pure geostrophic balance and therefore contain subtle conver-

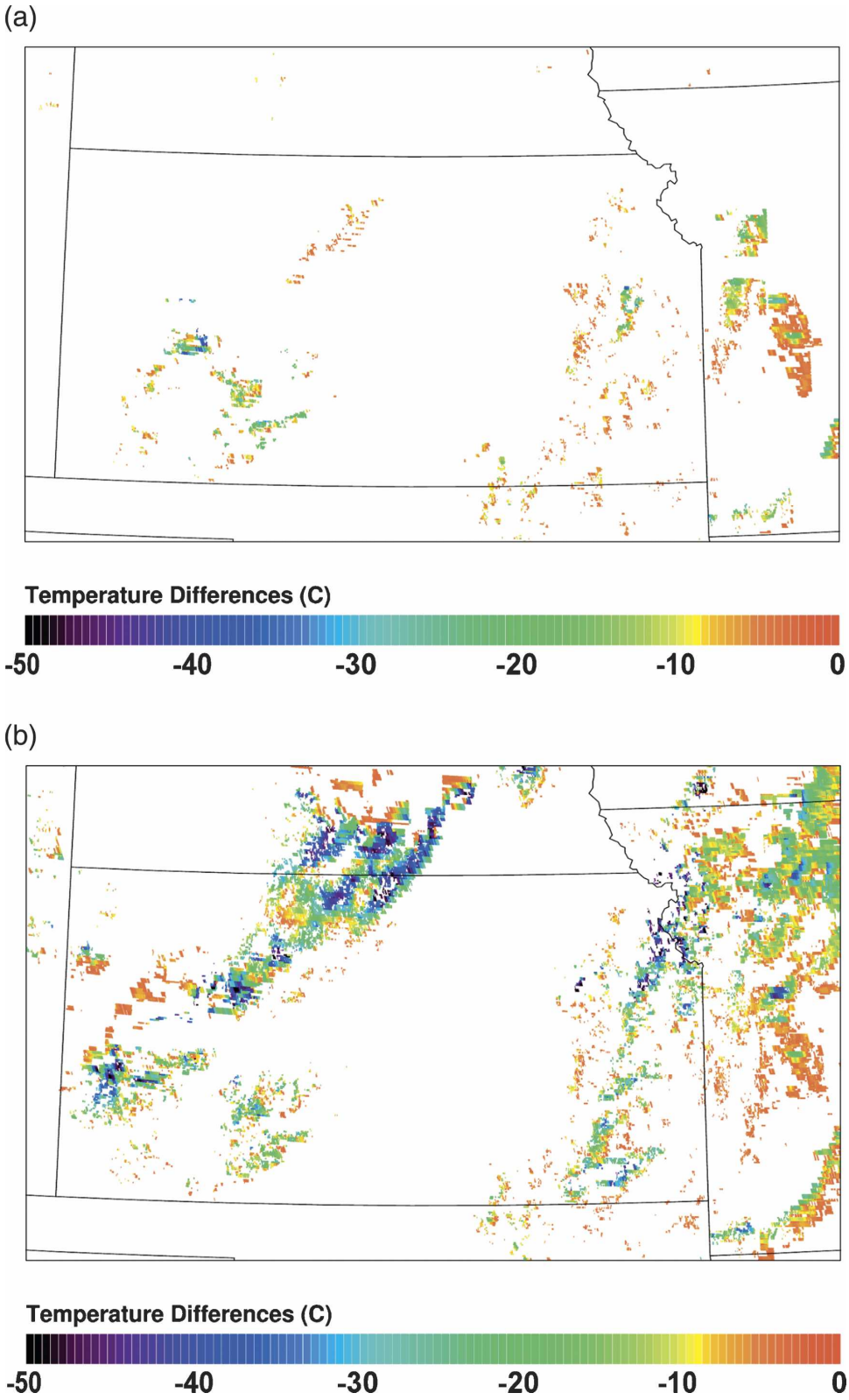

FIG. 8. A 30-min 10.7-μm cloud-top cooling estimate using (a) AMVs from typical operational processing settings and (b) mesoscale AMVs. Shown are temperature differences of less than −4°C.

gent and divergent flow components. AMVs that represent mesoscale flows are important in applications that monitor the rapid evolution of (convective) clouds in near–real time. A demonstration of cloud-top cooling estimates using mesoscale AMVs is performed for a CI event over Kansas. A comparison of mesoscale AMV-derived cooling estimates with those derived by a human expert yields very favorable results, thereby demonstrating the applicability of AMVs for CI nowcasting.

Acknowledgments. This research was supported by the NASA Advanced Satellite Aviation Weather Products (ASAP) award number 4400071484. The authors thank the anonymous reviewers for their feedback that helped to improve the quality of this work. The authors also thank the satellite-derived-winds group within the Cooperative Institute for Meteorological Satellite Studies at the University of Wisconsin—Madison for their help and guidance in installing the AMV identification software and advice for acquiring high-density AMV fields. The authors also thank Wayne Bresky for information regarding typical operational AMV processing settings. Special thanks are given to Chris Velden for providing a detailed review of this work and very constructive feedback.

REFERENCES

Barnes, S. L., 1964: A technique for maximizing details in numerical weather map analysis. *J. Appl. Meteor.,* **3,** 396–409.

Bonavita, M., and L. Torrisi, 2004: Use of satellite wind vectors in the Italian Weather Service numerical weather prediction system: Current status and perspectives. *Proc. Seventh Int. Winds Workshop*, Helsinki, Finland, WMO, 205–213. [Available online at www.eumetsat.de/.]

Cherubini, T., S. Businger, C. S. Velden, and R. Ogasawara, 2004: Assimilation of satellite-derived winds in mesoscale forecasts over Hawaii. *Proc. Seventh Int. Winds Workshop*, Helsinki, Finland, WMO, 215–224. [Available online at www.eumetsat.de/.]

Dunion, J. P., and C. S. Velden, 2002: Application of surface-adjusted GOES low-level cloud-drift winds in the environment of Atlantic tropical cyclones. Part I: Methodology and validation. *Mon. Wea. Rev.,* **130,** 1333–1346.

Fujita, T., 1968: Present status of cloud velocity computations from *ATS-1* and *ATS-3*. *COSPAR Space Res.,* **9,** 557–570.

Goerss, J. S., C. S. Velden, and J. D. Hawkins, 1998: The impact of multispectral *GOES-8* wind information on Atlantic tropical cyclone track forecasts in 1995. Part II: NOGAPS forecasts. *Mon. Wea. Rev.,* **126,** 1219–1227.

Hayden, C. M., and J. R. Purser, 1995: Recursive filter objective analysis of meteorological fields: Applications to NESDIS operational processing. *J. Appl. Meteor.,* **34,** 3–15.

Holmlund, K., 1998: The utilization of statistical properties of satellite-derived atmospheric motion vectors to derive quality indicators. *Wea. Forecasting,* **13,** 1093–1105.

Hubert, L. F., and L. F. Whitney Jr., 1971: Wind estimation from geostationary-satellite pictures. *Mon. Wea. Rev.,* **99,** 665–672.

Key, J., D. Santek, C. S. Velden, N. Bormann, J.-N. Thepaut, L. P. Riishojgaard, Y. Zhu, and W. P. Menzel, 2002: Cloud-drift and water vapor winds in the polar regions from MODIS. *IEEE Trans. Geosci. Remote Sens.,* **41,** 482–492.

LeMarshall, J. F., C. Spinoso, N. R. Pescod, and G. A. Mills, 1996: Estimation and assimilation of hourly high special resolution wind vectors based on *GMS-5* observations. *Aust. Meteor. Mag.,* **45,** 275–284.

——, N. Pescod, R. Seecamp, K. Puri, C. Spinoso, and R. Bowen, 1999: Local estimation of *GMS-5* water vapour motion vectors and their application to Australian region numerical weather prediction. *Aust. Meteor. Mag.,* **48,** 73–77.

Mecikalski, J. R., 2002: Using cloud-motion winds to understand kinematic processes of deep convection: Anvil-level outflow and momentum transport. *Proc. Sixth Int. Winds Workshop*, Madison, WI, WMO, 97–104. [Available online at www.eumetsat.de/.]

——, and K. M. Bedka, 2005: Forecasting convective initiation by monitoring the evolution of moving cumulus in daytime GOES imagery. *Mon. Wea. Rev.,* in press.

Menzel, W. P., and J. F. W. Purdom, 1994: Introducing GOES-I: The first of a new generation of geostationary operational environmental satellites. *Bull. Amer. Meteor. Soc.,* **75,** 757–781.

——, W. L. Smith, and T. R. Stewart, 1983: Improved cloud motion wind vector and altitude assignment using VAS. *J. Climate Appl. Meteor.,* **22,** 377–384.

Merrill, R. T., W. P. Menzel, W. Baker, J. Lynch, and E. Legg, 1991: A report on the recent demonstration of NOAA's upgraded capability to derive satellite cloud motion winds. *Bull. Amer. Meteor. Soc.,* **72,** 372–376.

Nieman, S. J., W. P. Menzel, C. M. Hayden, D. Gray, S. T. Wanzong, C. S. Velden, and J. Daniels, 1997: Fully automated cloud-drift winds in NESDIS operations. *Bull. Amer. Meteor. Soc.,* **78,** 1121–1133.

Rabin, R. M., S. F. Corfidi, J. C. Brunner, and C. E. Hane, 2004: Detecting winds aloft from water vapor satellite imagery in the vicinity of storms. *Weather,* **59,** 251–257.

Rao, P. A., C. S. Velden, and S. A. Braun, 2002: The vertical error characteristics of GOES-derived winds: Description and experiments with numerical weather prediction. *J. Appl. Meteor.,* **41,** 253–271.

Roberts, R. D., and S. Rutledge, 2003: Nowcasting storm initiation and growth using *GOES-8* and WSR-88D data. *Wea. Forecasting,* **18,** 562–584.

Sakamoto, M. S., H. Laurent, and L. A. Machado, 2004: The upper level winds and their relationship with convective systems: A case study. *Proc. Seventh Int. Winds Workshop*, Helsinki, Finland, WMO, 225–232. [Available online at www.eumetsat.de/.]

Schmetz, J., K. Holmlund, J. Hoffman, B. Strauss, B. Mason, V. Gartner, A. Koch, and L. van de Berg, 1993: Operational cloud-motion winds from Meteosat infrared images. *J. Appl. Meteor.,* **32,** 1206–1225.

——, and Coauthors, 1995: Monthly mean large-scale analyses of upper-tropospheric humidity and wind field divergence derived from three geostationary satellites. *Bull. Amer. Meteor. Soc.,* **76,** 1578–1584.

Soden, B. J., C. S. Velden, and R. E. Tuleya, 2001: The impact of satellite winds on experimental GFDL hurricane model forecasts. *Mon. Wea. Rev.,* **129,** 835–852.

Szejwach, G., 1982: Determination of semi-transparent cirrus cloud temperature from infrared radiance: Application to METEOSAT. *J. Appl. Meteor.,* **21,** 384–393.

Tokuno, M., 1996: Operational system for extracting cloud motion and water vapor motion winds from *GMS-5* image data. *Proc. Third Int. Winds Workshop,* Ascona, Switzerland, WMO, 21–30 [Available online at www.eumetsat.de/.]

Velden, C. S., and J. A. Young, 1994: Satellite observations during TOGA COARE: Large-scale descriptive overview. *Mon. Wea. Rev.,* **122,** 2426–2441.

——, C. M. Hayden, P. W. Menzel, J. L. Franklin, and J. S. Lynch, 1992: The impact of satellite-derived winds on numerical hurricane track forecasting. *Wea. Forecasting,* **7,** 107–119.

——, ——, S. J. Nieman, W. P. Menzel, S. Wanzong, and J. S. Goerss, 1997: Upper-tropospheric winds derived from geostationary satellite water vapor observations. *Bull. Amer. Meteor. Soc.,* **78,** 173–195.

——, T. L. Olander, and S. Wanzong, 1998: The impact of multispectral *GOES-8* wind information on Atlantic tropical cyclone track forecasts in 1995. Part I: Dataset methodology, description, and case analysis. *Mon. Wea. Rev.,* **126,** 1202–1218.

——, and Coauthors, 2005: Recent innovations in deriving tropospheric winds from meteorological satellites. *Bull. Amer. Meteor. Soc.,* **86,** 205–223.

Xiao, Q., X. Zou, M. Pondeca, M. A. Shapiro, and C. S. Velden, 2002: Impact of *GMS-5* and *GOES-9* satellite-derived winds on the prediction of a NORPEX extratropical cyclone. *Mon. Wea. Rev.,* **130,** 507–528.